OPEN ACCESS

University of BRISTOL

Yanagishima, T., Russo, J., & Tanaka, H. (2017). Common mechanism of thermodynamic and mechanical origin for ageing and crystallization of glasses. *Nature Communications*, *8*, [15954]. https://doi.org/10.1038/ncomms15954

Publisher's PDF, also known as Version of record

License (if available):
CC BY

Link to published version (if available):
10.1038/ncomms15954

Link to publication record in Explore Bristol Research

PDF-document

University of Bristol - Explore Bristol Research
General rights

ARTICLE

Common mechanism of thermodynamic and mechanical origin for ageing and crystallization of glasses

Taiki Yanagishima[1], John Russo[1,2] & Hajime Tanaka[1]

The glassy state is known to undergo slow structural relaxation, where the system progressively explores lower free-energy minima which are either amorphous (ageing) or crystalline (devitrification). Recently, there is growing interest in the unusual intermittent collective displacements of a large number of particles known as 'avalanches'. However, their structural origin and dynamics are yet to be fully addressed. Here, we study hard-sphere glasses which either crystallize or age depending on the degree of size polydispersity, and show that a small number of particles are thermodynamically driven to rearrange in regions of low density and bond orientational order. This causes a transient loss of mechanical equilibrium which facilitates a large cascade of motion. Combined with previously identified phenomenology, we have a complete kinetic pathway for structural change which is common to both ageing and crystallization. Furthermore, this suggests that transient force balance is what distinguishes glasses from supercooled liquids.

[1] Department of Fundamental Engineering, Institute of Industrial Science, The University of Tokyo, Komaba 4-6-1, Meguro-ku, Tokyo 153-8505, Japan.
[2] School of Mathematics, University of Bristol, Bristol BS8 1TW, UK. Correspondence and requests for materials should be addressed to H.T. (email: tanaka@iis.u-tokyo.ac.jp).

Ageing and devitrification are very slow dynamical processes taking place in glasses. Ageing leads to a gradual change in the physical properties of glasses[1,2]; a prominent example is a change in sample size, potentially very harmful for applications to high precision devices. Devitrification, the transformation of a glass to a crystal, has also been a subject of intensive study for many years[3]. For material scientists, the tendency for a supercooled system to devitrify during ageing or on heating can be detrimental to the stability of organic[4,5] and metallic glasses[6], silicates[7], macromolecules[8,9] and aqueous systems[10]. The latter is particularly relevant to cryogenics, where ice formation can have adverse effects on biological samples[11]. For many industrial products, including pharmaceuticals[4], devitrification during storage is also a very serious problem. Despite the technological importance of these phenomena, their fundamental mechanisms remain elusive, because of their slow dynamics and apparently stochastic nature.

To access the microscopic mechanisms behind ageing and devitrification, hard-sphere (colloidal) glasses provide an ideal system due to the experimental accessibility to particle-level information[12–16] and the simple nature of the hard-core interaction. Different studies have considered ageing and devitrification separately in hard-sphere glasses. In the case of ageing, an increase in structural order over time was found[17]. For hard spheres (both monodisperse and weakly polydisperse), structural order is characterized not only by density but also by bond orientational order (BOO), a measure of angular order between neighbouring particles. This ordering originates from a thermodynamic driving force to lower the free energy of the system. Note that higher BOO means larger vibrational (or correlational) entropy, that is, lower free energy for hard spheres (see, for example, ref. 18). Regarding devitrification, on the other hand, Pusey et al.[19] showed that crystallization can take place beyond the glass transition point in over-compressed hard-sphere glasses. This may apply more generally, as jammed or glassy metastable states are also seen to undergo ordering.

On deeper overcompression, Sanz et al.[20] found that crystallization occurs through discrete collective events, where groups of particles suddenly undergo large displacements, accompanied by an equally sudden increase in the proportion of crystalline particles in the system: these events were termed 'avalanches' for their intermittent, collective nature. They first found that the randomization of particle velocities in their molecular dynamics simulation averted the incidence of the events, and second, that polydispersity suppressed the growth of crystallinity while maintaining the same intermittent dynamics. Thus, they concluded that avalanches 'mediate' crystallization, or more precisely, that 'chance' collective motion in the system seemed to trigger the displacements that led to crystallization. At the same time, they noted that there was a spatial heterogeneity to which such events are linked, and suggested 'soft spots'[21] as a potential candidate for what might distinguish them from other regions. So while ageing is proposed to be thermodynamically driven[17], it is argued that devitrification and avalanche events are of a strongly stochastic nature with an unidentified structural signature for initiation; crystallization is their by-product. Thus, the connection between ageing and devitrification, if any, remains elusive: despite being the two principal dynamic phenomena taking place in glasses, their physical mechanisms also remain unknown. For example, what makes the kinetics of the phenomena in glasses special remains unclear, since the relation of ageing and devitrification to corresponding processes in the supercooled liquid state, that is, structural relaxation and crystallization, respectively, are yet to be ascertained.

Here, we address these fundamental problems by studying structural evolution during avalanches in both ageing and devitrifying hard-sphere systems. We show that ageing and devitrification are both characterized by the same kinetic processes, and that the special feature of dynamics in glasses originates from a temporal mechanical balance characteristic of solids, which has not been clearly recognized so far. We distinguish the very first particles to take part in avalanche events (AIs (avalanche initiator)) and go on to show that they are characterized by a structural signature, with a lower local density and low BOO. We then show that this motion leads to a transient loss in the force balance of the system, and it is this that gives rise to the cascade of particle motion which we perceive as an 'avalanche'. Finally, we find that this motion triggers displacements throughout the system in the vicinity of pre-ordered regions. We believe this to correspond to the avalanche devitrification identified by Sanz et al., though we go on to show that this happens in ageing systems as well.

Results

Progression of an avalanche. We simulate supercooled monodisperse and weakly polydisperse hard-sphere-like systems in the glassy regime to study devitrification and ageing, respectively. Details regarding the system and the simulation are given in the Brownian dynamics simulation section in the Methods. For the monodisperse case, we see a clear increase in the crystallinity, but not for the polydisperse case, as shown in Supplementary Fig. 1. We proceed to study how an avalanche event is triggered in a glass state, how this triggering event spreads over the system, or induces an avalanche, and how structural ordering is finally enhanced by the avalanche. We first observe the incidence and progression of avalanches, looking at the mean squared displacement (MSD) of particles in the system from some arbitrary time t_0. An example is shown in Fig. 1a for an ageing system. We can see that the sudden collective displacement of particles takes place intermittently. We proceed to look at the circled event in more detail in Fig. 1b. First, we identify four different times during the event: a time just preceding the event, t_i; the time at which the first particles are displaced and the MSD suddenly rises, t_a; an intermediate time t_m, purely for illustrative purposes; the time at which the MSD finally reaches its next plateau, t_f. Snapshots of the system at each of these times are given in Fig. 1c–f, with blue shaded regions corresponding to regions with high BOO parameter $Q_6 > 0.25$ (see the Structural analysis section in the Methods for the definition of BOO) at time t_i. Only particles which are displaced more than $\sigma_l/3$ (σ_l being the size parameter of particle l (see the Analysis of avalanche events section in the Methods)) between t_i and the time of the snapshot are shown.

Starting from a quiescent, metastable state in Fig. 1c, we see that a small, localized cluster of these particles appear in panel d. When the number of nearby particles displaced more than the $\sigma_l/3$ threshold becomes > 5 for the first time after time t_i, we call these particles AIs. These will be discussed at length below. Note that they appear in disordered regions with low local crystalline BOO (low Q_6). This is followed by particles in the vicinity being subsequently displaced, as shown in panel e, before the system reaches the next plateau at panel f. The avalanche particles identified at the end of the event are called APs, and, with few exceptions, are significantly more numerous than AIs.

Structural origin and evolution of AIs and APs. Note that we now have three populations of particles, AIs, APs and the whole set. These can be analysed separately with a large enough sample of events. With lists of AIs and APs over all the events, we go on to look at the typical local structure of AIs and APs at t_i. We start with local volume density ϕ_l, defined as $\frac{1}{6}\pi d_l^3 / V_{vor}^l$, where d_l is the
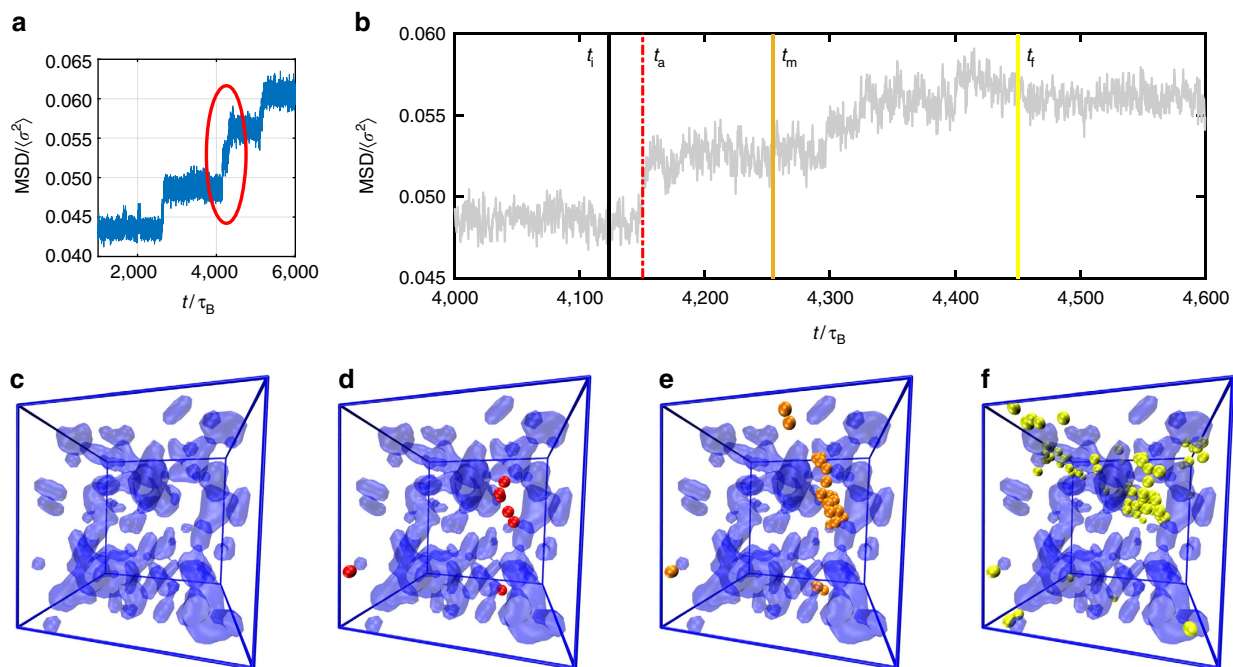
Figure 1 | Avalanche over time seen in an ageing system at $\phi = 0.65$. (**a**) MSD over all particles from a time t_0. We can see distinct avalanche events that happen intermittently. The circled event is the same as that shown in **c**–**f**. (**b**) MSD over all particles from a time t_0, focused on the avalanche event circled in **a**. Times t_i, t_a, t_m and t_f correspond to snapshots **c**–**f**, respectively. (**c**–**f**) Progression of the circled avalanche event in **a**. Blue shaded regions are regions where $Q_6 > 0.25$. We only display particles which have been displaced more than $\sigma_l/3$ since snapshot **c** in each panel. We can see the number of these particles increase progressively. Particles displayed at **d** can be regarded as AIs, whereas particles appearing later on are APs. All other particles are not displayed. Despite the step-like appearance of the MSD in **b**, it is reasonable to assume that this is one collective event, as we can see in **c**–**f**.

effective particle diameter (see the Brownian dynamics simulation section in the Methods) and V_{vor}^l is the local volume of particle l as found from a radical Voronoi tesselation. A distribution of ϕ_l values for AIs, APs and all particles at t_i, is shown in Fig. 2a,d for devitrifying and ageing systems, respectively. It is clear that AIs are found in regions with a markedly lower density than the global average. APs exhibit this to a much lesser extent.

A lower density can arise from either larger local Voronoi volumes or simply smaller particle size. In the monodisperse (devitrifying) case, only the former is possible, whereas both are possible for the polydisperse case. We look at the distribution of local Voronoi volumes for the polydisperse (ageing) case, only to find that the volume for AIs is in fact skewed towards lower values, that is, towards higher volume fraction, albeit only slightly. This is shown in Supplementary Fig. 2a, where the distributions of local Voronoi volumes are given for AIs, APs and all particles. The lower local volume fraction in the polydisperse case must thus come primarily from AIs having smaller particle size, as confirmed in the particle size distributions given in Supplementary Fig. 2b.

Similar intermittent dynamics have been reported for ageing in glasses in simulations and experiments[22–25]. These works identified avalanche events as barrier-crossing events in a complex energy landscape under the influence of internal stresses. In this energy-landscape picture, AIs and APs can be related to the activation stage (from the initial states to the nearby saddle states) and the relaxation stage (from the saddle states to the final states), respectively. Egami et al.[25] also found cascade events spreading over the whole system in unstable glasses formed by an instant quench, which may be caused by large-amplitude density inhomogeneities frozen in by such a quench. A link between such nonlocal events and self-organized criticality was also suggested[23,25], but it is beyond the scope of our paper. Here we focus on localized events in a rather stable glass, which is

crucial for identifying structural characteristics that are independent of the box size. This allows us to reveal a specific mechanism for event initiation, propagation and consequence.

Going on to look at BOO parameters Q_6 and w_6, we superimpose the values of these parameters for AIs and APs over all trajectories for devitrifying and aging cases over a typical distribution over the whole system at some arbitrary time point (Fig. 2b,e). Q_6 is associated with crystalline BOO in hard-sphere systems, while a lower (more negative) w_6 is associated with dodecahedral and icosahedral BOO[26]. It is clear that AIs can be found concentrated in regions where neither Q_6 nor $-w_6$ are notably large, that is, in disordered regions. The average value over the AIs is noted as a white square on each, both below the thresholds associated with crystals and locally favoured structures. The distribution of APs, on the other hand, are indistinguishable from the typical distribution.

From these two findings, we can conclude that avalanches are more likely to initiate from a low degree of structural order and a low local Voronoi density (see Fig. 3 on the correlation between the structural order and local density). This region may be regarded as a kind of 'defect' in a glass.

We look further, and see whether certain changes in translational order or BOO are more likely for AIs and APs compared to the population as a whole. This can be shown by calculating $p(\Delta O)_{subset} - p(\Delta O)_{whole}$, where O is the order parameter of interest. Looking at the devitrifying case first in Fig. 2c, we find several things. First, it is clear that both AIs and APs, with their large displacements, generally entail a greater change in the local volume fraction ϕ_l than average, giving the curves their distinctive 'cursive V' shape. AIs and APs are less likely to have a local volume fraction change $|\Delta\phi_l| < 0.04$ than average, and more likely to have a ϕ_l change > 0.04, with a maximum around $|\Delta\phi_l| \sim 0.06$. This implies that particles with large amplitude displacements are most likely accompanied by a
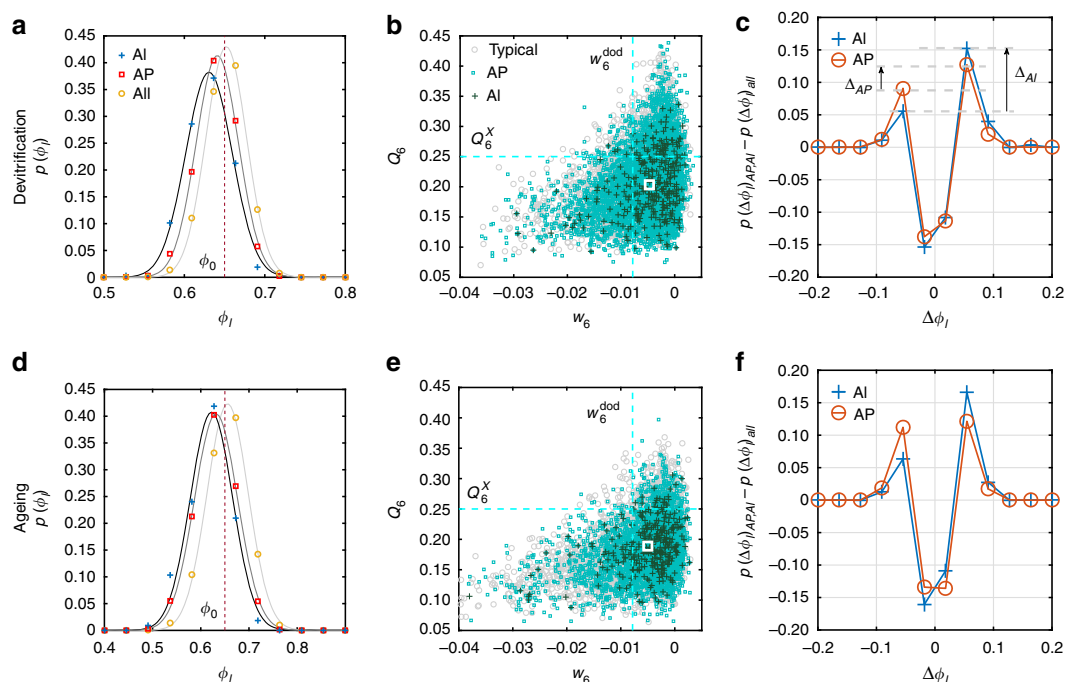
Figure 2 | Characterization of avalanche events. Averages are given over 50 events in both devitrifying and ageing events. (**a,d**) Distribution of local volume fraction ϕ_I before avalanche events. Both show a peak shift to lower ϕ_I for AIs, less so for APs. (**b,e**) w_6 and Q_6 distributions for AIs and APs (defined in text) overlaid on a typical distribution for all particles. The AIs especially are concentrated at lower BOO parameter values (both w_6 and Q_6). Dashed line Q_6^X and w_6^{dod} show the threshold values separating particles with highly crystal-like order ($Q_6 \geq Q_6^X$) and those with high dodecagonal or icosahedral-like order ($w_6 \leq w_6^{dod}$)[26]. Note that crystals have Q_6 larger than 0.4 (see the Structural analysis section in the Methods for details). The white thick open square represents the average values of w_6 and Q_6 for AIs. On average, thus, AIs possess neither significant crystalline order nor locally favoured structures. This indicates that AIs are particles localized in disordered regions. (**c,f**) Difference between the probabilities of $\Delta\phi_I$ for AI or AP subsets and the distribution for the system as a whole. There is a bias towards larger change for both AIs and APs, but there is a skew to positive change for AIs which is not seen for APs. For both devitrification and ageing, APs almost equally gain or lose density, but AIs have a strong tendency to increase local density.

local volume change of magnitude ~ 0.06 under dense packing. Second, we note that the AIs are very clearly skewed towards an increase in local volume fraction ϕ_I. What is particularly interesting is that this feature is not observed for APs, that is, they are equally likely to find a positive and negative local volume change. We will show later that this is a direct consequence of the fact that the motion of APs is of mechanical (not thermodynamic) origin. Looking to the ageing case in Fig. 2f, we once again see this asymmetry for AIs and APs. The statistical robustness of these results is discussed in the Event statistics section in the Methods.

It is worth noting that local-structural order and local density are not entirely independent of each other at such a high packing density[18]. We are clearly in a regime where translational ordering and bond orientational ordering are closely related to each other, particularly for hard-sphere-like systems, where the local symmetry is selected by packing. Instead of looking at the structure at t_i, we now look at the change in local volume fraction ϕ_I and BOO over the time interval $t_i < t < t_f$ for the three subsets, starting with AIs. To sharpen the sensitivity of the BOO parameter to localized change, we choose q_6 instead of its coarse-grained counterpart Q_6. As seen in Fig. 3a,b, we see a positive correlation between an increase in q_6 and ϕ_I. Note that the colour map simply reflects the number of particles in the plot for particular $\Delta\phi$ and Δq_6 ranges. It should be noted that the trend is much stronger for the devitrifying case.

As seen in Fig. 2, AIs originate from regions of lower local volume fraction (or, density) and low BOO. Thus, the increase in ϕ_I is not so much a densification beyond the system average, but rather a relaxation of a density inhomogeneity present in the

heterogeneous, over-compressed structure. The causal relationship between them is clearly highlighted by the difference in the degree of asymmetry seen between AIs and APs. Since AIs have a structural origin, their states before and after are distinct. There is thus a clear structural distinction between AIs and APs: the asymmetry in structural evolution of AIs indicates the presence of a local, thermodynamic driving force for the initiation of avalanche events. On the other hand, it would appear that APs are rather a kinetic by-product of the AIs (discussion continued below). Here, it is worth noting that it is known[27] that there is no discernible difference between the distributions of Voronoi volumes and mobility for a supercooled liquid: it is our ability to identify AIs and APs that uncovers this structural distinction.

These conclusions are further confirmed for the monodisperse case by using an iso-configurational ensemble. We produced an iso-configurational ensemble ($\sim 2{,}000\tau_B$ length), initiated from a configuration taken from one of the many MSD plateaux in the monodisperse case. A total of 100 trajectories were found, and 38 events were recorded. Further to reproducing the spatial heterogeneity identified in ref. 20, we apply the same treatment as above to produce Fig. 4a–c: the trends are exactly the same as what was found for 50 independent trajectories. As seen in Fig. 4d, there is good agreement between the unique AIs (yellow) and regions which obey all of the following criteria: $Q_6 < 0.25$, $w_6 > -0.01$, $\phi_I < 0.62$, where the AI ϕ_I probability distribution becomes larger than the distribution over the whole system. Low density and low BOO thus provide us with the regions where AIs are more likely to appear, as they are characterized by lower activation energies for particle motion, where the caging effect is locally weaker. As in any stochastic process, the study of regions
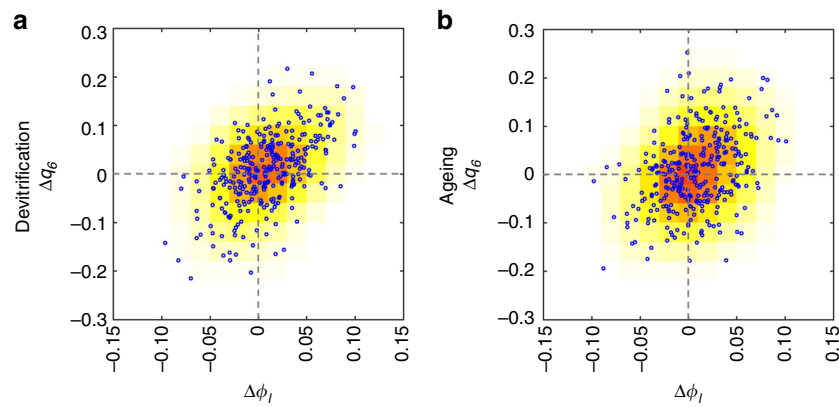
Figure 3 | Correlation between $\Delta\phi_l$ and Δq_6. Distribution of $\Delta\phi_l$ and Δq_6 for AIs for (**a**) Devitrification, (**b**) Ageing. There is a clear positive correlation between translational and orientational order at this depth of overcompression ($\phi = 0.65$).
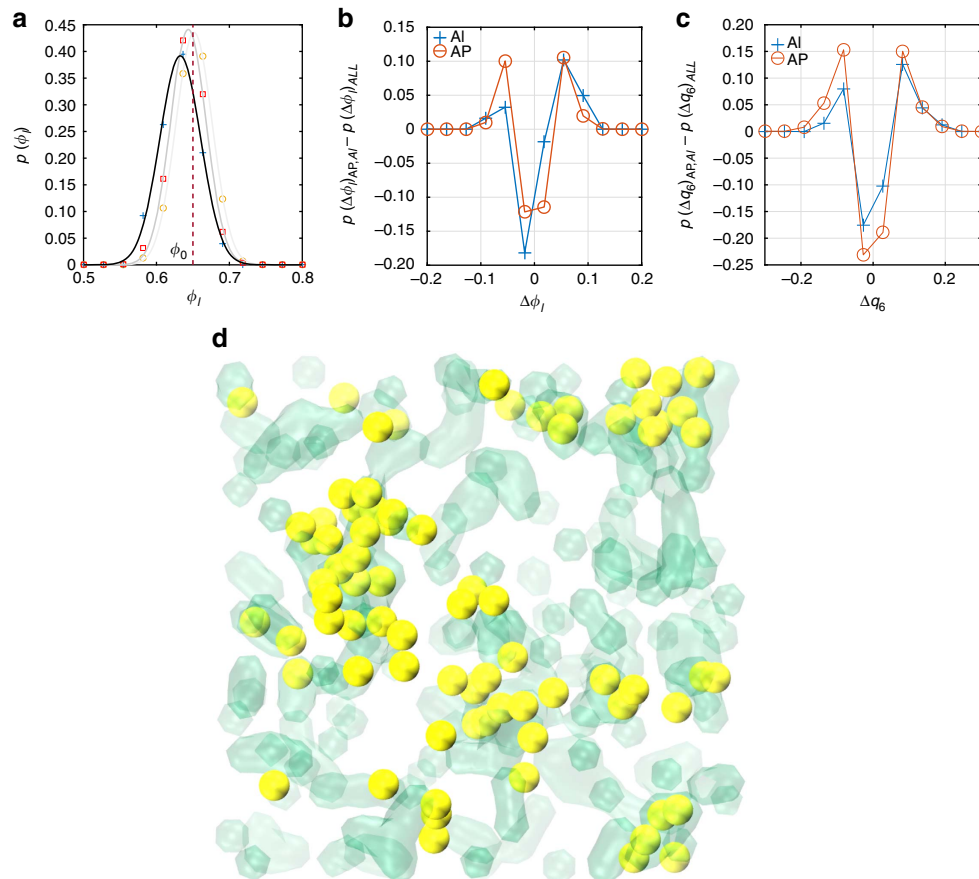

Figure 4 | Iso-configurational ensemble. Analysis of 38 events found in 100 iso-configurational trajectories for the monodisperse case ($\phi = 0.65$). The initial state is taken from one of the MSD plateaux in the original 50 independent runs. (**a**) Local Voronoi density distribution for AIs, APs and all particles, and differences between all-particle probability distributions and AI, AP distributions for changes in (**b**) local density ϕ_l and (**c**) BOO parameter q_6. Data is given for the monodisperse set. Note that all prominent features of the independent runs are replicated, including a lower initial local density and marked asymmetry in structural change for AIs, and not for APs. (**d**) A map of all unique AIs (yellow) from the detected events and regions (transparent green) which fulfil all of the following conditions: $Q_6 < 0.25$, $w_6 > -0.01$, $\phi_l < 0.62$.

of low density and low BOO order only provides a probability map of where AIs will occur. The actual location cannot be predicted in a deterministic way, as the underlying motion is Brownian, without memory effects (inertia).

Function of APs in structural evolution. Does this mean that APs do not have any role to play in crystallization or ageing? If the only significant structural evolution in the system was derived

from the AIs, the total change would be minuscule, as AIs associated with an event make up only around 0.2–0.3% of the system (~ 10 particles in 4,000). Consider the events shown in Fig. 5, where panels a and c are events from devitrifying and ageing trajectories, respectively. Yellow particles are AIs and red particles are APs. In panel a, dark blue particles are particles which are crystalline at t_i, and light blue particles are those that become crystalline by t_f. In panel c, blue particles are those with
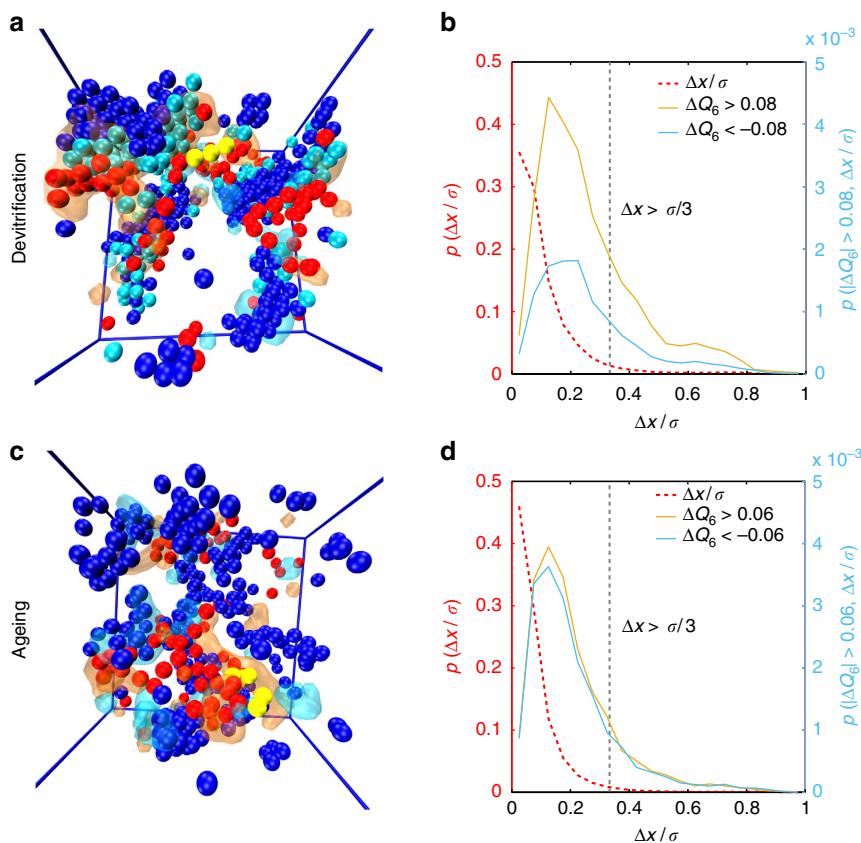
Figure 5 | Displacement and structural change. (**a**) Spatial distribution of crystalline (blue), newly crystalline (light blue), AIs (yellow) and APs (red) during an avalanche event in the monodisperse case at $\phi = 0.65$. Regions which have experienced a large change in BOO, $\Delta Q_6 > 0.08$ and $\Delta Q_6 < -0.08$, are marked with a transparent orange and cyan region, respectively. (**b**) Fraction of particles with displacement $\Delta x/\sigma$ for particles experiencing a large change in BOO parameter Q_6 during avalanches for monodisperse and polydisperse cases respectively. The red dashed curve is for all particles (left axis), whereas the orange and cyan curves are for particles experiencing a large positive and negative change in Q_6 respectively (right axis). The threshold is the same as in **a**. (**c**) The spatial distribution of MRCO regions (blue), AIs (yellow) and APs (red) during an avalanche event in the polydisperse case at $\phi = 0.65$. Regions which have experienced a large change in BOO, $\Delta Q_6 > 0.06$ and $\Delta Q_6 < -0.06$, are marked as a transparent orange and cyan region, respectively. (**d**) Same as b for the ageing case. The threshold is the same as in **c**. Note that the peaks in both **b**,**d** occur at displacements smaller than the avalanche threshold, $\Delta x > \sigma/3$, for particles experiencing a large change in Q_6.

$Q_6 > 0.25$. Orange and blue transparent clouds are regions with a pronounced increase or decrease in Q_6, respectively, thresholded at 0.08 in panel a and 0.06 in panel c. It is clear that the incidence of APs causes a significant amount of structural change in different parts of the system, particularly in the vicinity of pre-ordered clusters: importantly, regions where the largest BOO development is seen are not necessarily clustered around the AIs or APs.

This last point is worth considering carefully. Though there is some overlap, the particles which in fact experience the largest change are those which move less than the avalanche threshold, but more than average. Figure 5b,d show the fraction of particles with a particular displacement size for particles undergoing a large change in Q_6, for monodisperse and polydisperse cases, respectively, using the same thresholds for Q_6 changes as in panels a and c. The distribution of displacements for particles which undergo large structural change are peaked below the avalanche threshold, $\Delta x > \sigma_l/3$. This is not simply a reflection of the overall distribution of displacements in the system (see the red dashed curve), which has no peak and monotonically decreases with an increase in the displacement. Also note that there is a clear bias towards positive changes (orange curve) in Q_6 compared to negative changes (blue curve) for the devitrifying case.

In the above we have shown that APs are not the particles which crystallize, as also reported in ref. 20. In the final stage of

the avalanche identified in our work, APs cause movements which are smaller than the avalanche threshold and yet induce significant BOO development. This raises the fundamental question of what is the physical mechanism behind the avalanche mediated devitrification[20] in monodisperse systems, or why such small particle displacements (less than the particle size) can facilitate crystallization. The natural answer to this question arises from a crystallization pathway where the first step is development of spatial coherency in BOO and the fact that small displacements are enough for this enhancement[28]. On noting that enhancement of BOO spatial coherency cannot induce translational ordering in systems with a high enough polydispersity[18], we can now also claim the same mechanism for ageing systems.

In supercooled liquid and glassy states with weak frustration against crystallization, like the one studied here, the system always seeks a way to lower the free energy even at a local scale by using every possible kinetic path. In a glassy state, a system tries to increase structural order locally, which results in density inhomogeneities accumulated in the disordered region overcoming the energy barrier to motion (AIs), causing a cascade of particle motion (APs).

Intermittent dynamics and mechanical equilibrium. Having ascertained the structural origins of avalanche initiation, an

important question arises: what are the conditions underlying the intermittency of the dynamics? In an ordinary supercooled liquid, particle motion proceeds in a continuous manner. It is only in a highly supercooled or glassy state that we see intermittent, avalanche-like particle motion. We argue that the latter is a characteristic of a glassy state, where mechanical equilibrium is satisfied both locally and globally, at least transiently. Suggestions have been made[29,30] and evidence given[31,32] that mechanical balance is attained in a glassy state or in the inherent structure, resulting in the emergence of a long-range elastic correlation like in jammed granular matter[33]. Before an avalanche, a system is in a mechanically stable state even with thermal noise: the local ordering events which trigger the motion of AIs lead to the breakdown of this transient mechanical equilibrium, or the loss of force balance, until the system attains a new mechanically stable state.

Evidence for this in our system is given in Fig. 6, where we look at how particles change their neighbours over time. We can define two types of neighbour, simply using proximity (nearest neighbours, NNs) or those with which a repulsive force is acting (force neighbours, FNs). The average number of neighbours kept compared to some initial time is shown in Fig. 6a, both for FNs and NNs, superimposed on the progression of an avalanche event in a polydisperse trajectory. We can immediately see that the system is in a state of mechanical equilibrium before, with an extended plateau over which particles keep its neighbours, and maintains the force chain structure of the system. It is only when the avalanche initiates that this structure changes. The existence of a clear plateau afterwards shows that mechanical equilibrium has been restored, with a different connectivity between particles as before.

The best evidence for the role of mechanical stability is spatial correlation between AIs/APs and new FN connections. This is shown in Fig. 6c, where new force connections formed over the course of an avalanche have been shown as bold red bonds, superimposed on transparent blue bonds representing the original force network before the event. The AIs (yellow) and APs (red) for the event are also shown. The abrupt formation of these new FNs is also shown dynamically in the Supplementary Movie.

It is worth noting that the average number of FNs surrounding AIs and APs is around 6, the Maxwell rigidity criterion[34] in three dimensions. Distributions for the number of FNs for AIs, APs and all particles for both monodisperse and polydisperse cases are given in Supplementary Fig. 3. The role of this in the dynamics becomes clearer when different volume fractions are considered. Short trajectories are produced for volume fractions ϕ ranging from 0.58 to 0.66 using the same number of particles n, and the average number of FNs recorded after $t \approx 300\tau_B$. It can be seen that the average number of FNs, $\bar{n}_{FN}$, first passes this threshold when the volume fraction reaches $\phi = 0.65$ (Fig. 6b). This coincides with the volume fraction above which the avalanches can be observed, that is, sudden jumps are seen in the MSD preceded and followed by clear plateaus (see Supplementary Fig. 4). Also note that the increase in $\bar{n}_{FN}$ starts from the nominal glass transition volume fraction, $\phi_g \approx 0.58$–0.59 (Fig. 6b), corroborating the role that mechanical contacts might have to play in glass formation.

Note that the frequency of these jumps also changes with volume fraction. Avalanche events take place in an intermittent manner when a system is able to overcome the barrier between one metastable basin and another with the help of thermal noise. Since the height of this barrier steeply increases with an increase in the degree of supercooling, the frequency of avalanches should decrease for deeper supercooling; we confirm this in our simulations, as shown in Supplementary Fig. 4, where avalanche incidence is increasingly suppressed at higher volume fractions. This trend is also seen qualitatively in ref. 35 using a much sharper inter-particle potential.

Discussion

We have now seen that avalanche initiation has a structural precursor, and that the propagation of APs and the intermittency of the dynamics is related to the temporary loss of mechanical stability of the system for both devitrifying and ageing systems. Avalanches further induce small-amplitude motion of particles ($<\sigma_l/3$) in regions which already have a high structural order. It is however worth noting what makes the devitrifying and aging systems different. In the devitrifying systems considered here, the crystal growth is interface-limited, meaning that the barrier for crystallization comes from the addition of particles to the crystalline surface. This process does not require large-scale translational motion[28,36,37], and can thus occur under the small-amplitude motion set in place by AP particles. In most ageing systems (mixtures or highly polydisperse samples), crystal growth is instead diffusion-limited, thus requiring large-scale diffusional motion for the interface to grow, and it is thus not easily activated by avalanche motion. This is shown by the fact that particles undergoing large changes in BOO for the polydisperse case do not seem to reflect the clear bias to positive changes in q_6 seen in the monodisperse case, as shown in Fig. 5b,d. This is also evident for AIs and APs in Supplementary Fig. 5a,b, where there is no clear bias to order development like in Fig. 2c,f. These show that BOO development in ageing systems is not in the expected thermodynamic direction for every event. Of the 50 polydisperse runs, 32 cases experience an overall increase in Q_6, the others experience a decrease. There is, however, an overall positive trend: the mean change in Q_6 per event is $\Delta Q_6 = (2.24 \pm 1.94) \times 10^{-4}$, where the error is an unbiased standard error in $\Delta \bar{Q}_6$. This corresponds to $\approx 87\%$ confidence in a Q_6 increase. This is in contrast to a $\Delta Q_6 = (3.83 \pm 1.39) \times 10^{-4}$ for the monodisperse case, with a 99.8% confidence in a Q_6 increase. This bias to positive changes reflects the thermodynamic direction, which is hindered by the suppression of long-range diffusion in the polydisperse case.

As seen in Fig. 5c, regions where large changes in BOO occur are localized to pre-ordered regions (MRCO). Previous work on ageing in 3D hard-sphere systems at lower volume fractions[17] has shown that there is a slow development in the spatial correlation length of BOO parameter Q_6. Such an increase is most easily achieved if re-structuring takes place near pre-ordered sites, explaining the large changes in Q_6 close to MRCO regions induced by nearby AP motion. This is analogous to the localization of Q_6 growth to the MRCO in the devitrifying case, with an added stochasticity factor.

Finally, we give evidence for the fact that APs form strings, as briefly noted in ref. 20. Supplementary Fig. 6 shows the degree of overlap with the former position of neighbours at an arbitrarily chosen initial point over time, a decrease in which denotes string-like displacement. The exact definition is given in the String-like collective motion section in the Methods. The event is the same as the one used in Fig. 6a; the coincidence with avalanche incidence is clear. It is particularly interesting that the collective, string-like motion seen in the Adam–Gibbs scenario for quasi-equilibrium supercooled liquids[38] could be involved in the structural evolution of the glassy state of unstable glasses like the ones shown here. String-like motion may be the only possible way for particles to move in a highly packed state[38]. This similarity in dynamics lends further credence to a thermodynamic picture of the glass transition and the intrinsic link between crystallization and vitrification under the influence of frustration[18].
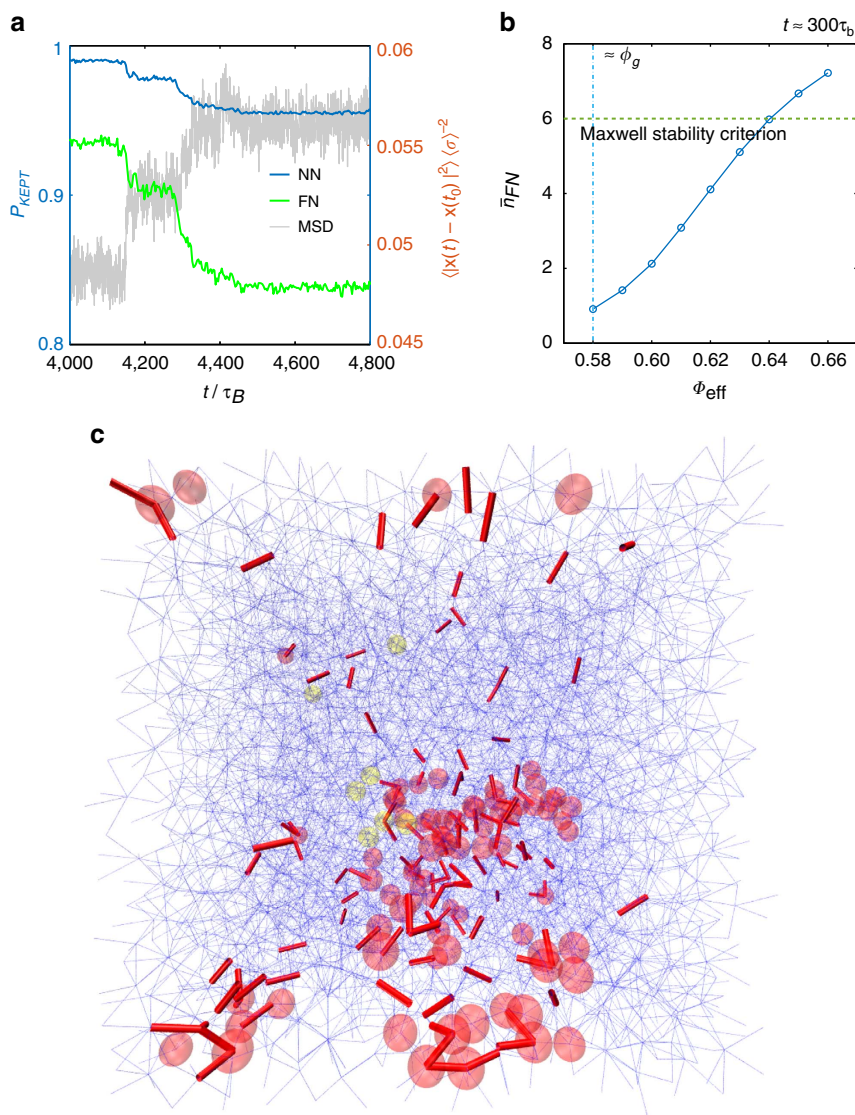
Figure 6 | Breakage of force chains. (**a**) The average proportion of neighbours kept by particles (left axis) compared to its neighbours at some initial time preceding an avalanche event in a polydisperse trajectory ($\phi = 0.65$). Results are shown for both nearest neighbours (NNs: blue curve) and force neighbours (FNs: green curve). The mean-squared displacement of the system is shown in the background by a grey curve (right axis): the re-arrangement of the system force network coincides with the avalanche. (**b**) The average number of FNs, $\bar{n}_{FN}$, observed after $300\tau_B$ at different volume fractions. (**c**) Re-arrangement of the force network during the avalanche event shown in **a**. Yellow and red particles are AIs and APs respectively, as in Fig. 5a,c. The stable force network that is not involved in the re-arrangement is shown by the blue network, whereas newly formed force bonds resulting from a re-arrangement since a time preceding the avalanche are shown as thick red bonds. We can see some correlation between APs and AIs and a significant local re-arrangement of FNs. This is a snapshot after an avalanche event; please see the Supplementary Movie to see the correlation over the course of the whole event.

The emerging picture of an avalanche in glasses is thus the following. Avalanches occur between mechanically stable states, where the force network between particles does not change with time. They are initiated by small clusters of particles (AIs) that have lower than average local density, within environments with a low crystalline BOO, a lack of locally favoured structures (icosahedra), and where the number of constraints is close to the threshold for mechanical stability. In polydisperse systems, AIs are more often small particles. Due to the loss of mechanical stability, the displacement of the AIs is propagated through the system in a cascade-like fashion; these particles are called APs and, on average, do not directly experience distinct structural evolution, that is, locally, they will almost equally likely decrease or increase the amount of crystalline order in the system, although slightly biased towards the increase. This makes them

unique from AIs. However, the APs induce significant change in their surroundings which move less, but cause a development of Q_6 in the vicinity of nearby highly ordered clusters. This triggering of ordering is analogous to the crystallization of supercooled liquids under some external perturbation. In short, we find that the ageing and devitrification of glasses proceed via a common pathway involving the interplay of thermodynamics and mechanics: thermodynamically-initiated mechanical facilitation of particle motion (that is, avalanche) and the enhancement of structural order by the cascade of small-scale displacements induced by this avalanche event.

This work highlights a kinetic pathway via which strongly supercooled glassy systems can age or devitrify, highlighting the particular role that inhomogeneities in density and structural order have to play in their stability—a stronger frustration

towards this kind of relaxation would make a glassy state more stable against ageing or devitrification. This is a useful guiding principle for the stabilization of the amorphous state in various materials. For a multi-component glass, for example, local demixing is required for devitrification. The mechanism of devitrification in such a mixture remains for future investigation.

Methods

Brownian dynamics simulation. We simulated supercooled monodisperse and weakly polydisperse glasses in the glassy regime using Brownian dynamics simulation for particles interacting through a Weeks–Chandler–Andersen (WCA) potential[39] in a three dimensional box with periodic boundary conditions. We employed the monodisperse system as an example of a devitrifying system and a weakly polydisperse system (6% Gaussian) as an example of an ageing system[40]. The difference between them is clearly shown in Supplementary Fig. 1, where the proportion of crystalline particles p_X (see below) is shown over time. The devitrifying system experiences growth in crystallinity, whereas the ageing system does not.

Initial over-compressed states were attained using rapid compression, expanding the size of the particles from 1% their intended size to their final dimension in less than a Brownian time τ_B, including noise to allow frustration limited structures to relax. This is similar to the Lubachevsky–Stillinger algorithm[41]. Although this volume fraction exceeds random close packing fraction ($\sim$64% and $\sim$66% for monodisperse and polydisperse cases, respectively[18]), local-structural ordering such as BOO allows a system to retain mobility. We note that the volume fraction is well above the glass transition volume fraction ($\phi_g \sim 0.58$–0.59) and structural relaxation in the system, including the time scale of avalanches, would be significantly longer than the Brownian time τ_B. As our primary interest is in persistent changes in structure as opposed to transient fluctuations, we average all positions and BOO parameters over $3\tau_B$ intervals.

A Brownian Dynamics simulation code was developed in FORTRAN 95 using the Ermak–McCammon algorithm[42], with no hydrodynamic interactions and no inertial term. Particles interact via a WCA potential, $U_{WCA}(r) = 4\epsilon\{(\sigma/r)^{12} - (\sigma/r)^6 + 1/4\}$ for $r < 2^{\frac{1}{6}}\sigma$, where σ is the diameter of the particle, and the temperature kept such that $k_B T/\epsilon = 0.025$ (k_B being the Boltzmann constant), as in refs 17,43. Volume fractions are calculated using an effective diameter $d = 1.0953\sigma$ where the WCA potential decays to $k_B T$. This is in agreement with a mapping of the WCA potential phase diagram to the hard sphere one to within $<0.5\%$ (ref. 44). The diffusivity D is chosen to mimic experimental colloidal systems, assuming a 1 μm particle radius in aqueous viscous surroundings with a viscosity of 1 mPas.

For all simulations shown in the main text, the number of particles is $n = 4,000$ unless otherwise stated. Here we mention the dependence of the observed dynamics, particularly the MSD, on system size. We produced eight trajectories with a system size $n = 16,000$, and compared their MSDs with eight randomly chosen trajectories from the $n = 4,000$ set in the monodisperse case. This is given in Supplementary Fig. 7. It can be seen that events are smaller and less well-defined for larger system size. This is to be expected, since the properties of individual events should be independent of system size, that is, since the MSD is normalized by particle number, and the events give smaller jumps in the MSD. Also, a larger system size makes it more likely for multiple events to be occurring at once, hence the lack of clear, flat plateaux, as events initiate before APs from another event have relaxed.

Structural analysis. The metrics we employ include local density as characterized by a radical Voronoi construction, and the q_6 order parameter which has found wide acceptance as a suitable order parameter to detect crystalline order in hard spheres[45,46]. Five-fold symmetric structures, such as icosahedral and dodecahedral structures, are targeted with the w_6 order parameter[26]. BOO parameters such as q_6 and w_6 are calculated as described in ref. 47. To reduce fluctuations in the distribution of q_6, a coarse-grained version, commonly written as Q_6, is also employed[48]. All the definitions of the order parameters can be found in ref. 28. Here we note that crystals have Q_6 larger than 0.4 (refs 45,49). The proportion of crystalline particles p_X is defined as the proportion of particles in the system which have seven or more 'solid' bonds, that is, bonds between NNs for which the bond coherence $d_{6ij} = \mathbf{q}_6(i) \cdot \mathbf{q}_6(j)/|\mathbf{q}_6(i)||\mathbf{q}_6(j)|$ (ref. 28) exceeds 0.7. Radical Voronoi constructions were carried out using the VORO++ package available at http://math.lbl.gov/voro++/ (ref. 50).

Analysis of avalanche events. We analyse three populations of particles, AIs, APs and the whole set, with a large enough sample of events as follows. In 32 independent simulations of devitrifying and ageing systems, each $\sim$7,000τ_B in length, we identified 50 avalanche events each for both cases. Care was taken to identify events which had a clear beginning and end, that is, with a clear plateau in the mean-squared displacement at both ends. Each event was labelled manually with a t_i and t_f and APs were found by comparing the state of the system at these two times; AIs for each event were found by comparing particle positions for progressively later times from t_i until the condition above was met.

Event statistics. We briefly comment on the statistics of this result. Histograms were generated by taking probability distributions over AIs, APs and all particles for individual events and then averaging these, avoiding bias of data to larger events among the 50 that were identified. The marker size (in both Fig. 2c,f and Supplementary Fig. 5a,b) is an indication of the maximum contribution possible from each event. In total, 315 AIs and 6,121 APs were counted for the monodisperse case, 320 AIs and 3,718 APs for the polydisperse case. Given the relatively small number of AIs, the width of bins could not be made significantly narrower than what is shown. To be sure that these trends are not due to some particularly favourable events mixed into the set, we focused on the two peaks in Fig. 2c,f, took a random selection of 25 events amongst the sets of 50, and measured the asymmetry between the AI and AP curves, marked Δ_{AI} and Δ_{AP} in the figure. This was repeated 100 times. In the monodisperse case, $\Delta_{AI} = 0.0976 \pm 0.0235$ and $\Delta_{AP} = 0.0384 \pm 0.0148$; in the polydisperse case, $\Delta_{AI} = 0.1044 \pm 0.025$ and $\Delta_{AP} = 0.0099 \pm 0.0108$. In both cases, $\Delta_{AI} > \Delta_{AP}$.

String-like collective motion. Following the formalism of Donati et al.[38], we calculate the value of the collective motion parameter $\delta = \sigma_{ij}^{-1} \min(|\mathbf{X}_i(t) - \mathbf{X}_j(t_0)|, |\mathbf{X}_j(t) - \mathbf{X}_i(t_0)|)$, averaged over NNs i and j, and then over all particles in the system over time. σ_{ij} is the sum of the radii of particles i and j. Here $\mathbf{X}_i$ is the position vector of particle i. The original work set a threshold for δ below which strings were considered to move collectively. Thus, we can interpret a decrease in the global average value of δ to be a collective displacement. As shown in Supplementary Fig. 6 (same polydisperse trajectory as in Fig. 6a), the global value of δ decreases during the course of an avalanche, with well-defined metastable states before and after.s

Data availability. The raw data analysed to derive the findings of this paper is available from the corresponding author upon reasonable request.

References

1. Struik, L. C. E. *Physical Aging in Amorphous Polymers and Other Materials* (Elsevier, 1978).
2. Kob, W. Computer simulations of supercooled liquids and glasses. *J. Phys. Condens. Matter* **11,** R85–R115 (1999).
3. Kelton, K. F. & Greer, A. L. *Nucleation in Condensed Matter: Applications in Materials and Biology* vol. 15 (Elsevier, 2010).
4. Craig, D. Q. M., Royall, P. G., Kett, V. L. & Hopton, M. L. The relevance of the amorphous state to pharmaceutical dosage forms: glassy drugs and freeze dried systems. *Inter. J. Pharm.* **179,** 179–207 (1999).
5. Powell, C. T. *et al.* Fast crystal growth from organic glasses: comparison of o-terphenyl with its structural analogs. *J. Phys. Chem. B* **118,** 8203–8209 (2014).
6. Greer, A. L. Metallic glasses. *Science* **267,** 1947–1953 (1995).
7. Marshall, R. R. Devitrification of natural glass. *Geol. Soc. Am. Bull.* **72,** 1493–1520 (1961).
8. Sear, R. P. Nucleation: theory and applications to protein solutions and colloidal suspensions. *J. Phys. Condens. Matter.* **19,** 033101 (2007).
9. Doye, J. P. K. *et al.* Controlling crystallization and its absence: proteins, colloids and patchy models. *Phys. Chem. Chem. Phys.* **9,** 2197–2205 (2007).
10. Angell, C. A. Liquid fragility and the glass transition in water and aqueous solutions. *Chem. Rev.* **102,** 2627–2650 (2002).
11. Mazur, P. Freezing of living cells: mechanisms and implications. *Am. J. Physiol.* **247,** C125–C142 (1984).
12. Weeks, E. R., Crocker, J. C., Levitt, A. C., Schofield, A. & Weitz, D. A. Three-dimensional direct imaging of structural relaxation near the colloidal glass transition. *Science* **287,** 627–631 (2000).
13. Gasser, U., Weeks, E. R., Schofield, A., Pusey, P. N. & Weitz, D. A. Real-space imaging of nucleation and growth in colloidal crystallization. *Science* **292,** 258–262 (2001).
14. Simeonova, N. *et al.* Devitrification of colloidal glasses in real space. *Phys. Rev. E* **73,** 041401 (2006).
15. Lynch, J. M., Cianci, G. C. & Weeks, E. R. Dynamics and structure of an aging binary colloidal glass. *Phys. Rev. E* **78,** 031410 (2008).
16. Yunker, P., Zhang, Z., Aptowicz, K. B. & Yodh, A. G. Irreversible rearrangements, correlated domains, and local structure in aging glasses. *Phys. Rev. Lett.* **103,** 115701 (2009).
17. Kawasaki, T. & Tanaka, H. Structural evolution in the aging process of supercooled colloidal liquids. *Phys. Rev. E* **89,** 062315 (2014).
18. Tanaka, H. Bond orientational order in liquids: towards a unified description of water-like anomalies, liquid-liquid transition, glass transition, and crystallization. *Eur. Phys. J. E* **35,** 113 (2012).
19. Pusey, P. N. *et al.* Hard spheres: crystallization and glass formation. *Philos. Trans. R. Soc. A* **367,** 4993–5011 (2009).
20. Sanz, E. *et al.* Avalanches mediate crystallization in a hard-sphere glass. *Proc. Natl Acad. Sci. USA* **111,** 75–80 (2014).
21. Widmer-Cooper, A., Perry, H., Harrowell, P. & Reichman, D. R. Irreversible reorganization in a supercooled liquid originates from localized soft modes. *Nat. Phys.* **4,** 711–715 (2008).

9

22. El Masri, D., Berthier, L. & Cipelletti, L. Subdiffusion and intermittent dynamic fluctuations in the aging regime of concentrated hard spheres. *Phys. Rev. E* **82,** 031503 (2010).

23. Vollmayr-Lee, K. & Baker, E. A. Self-organized criticality below the glass transition. *Europhys. Lett.* **76,** 1130–1136 (2006).

24. Evenson, Z. *et al.* X-ray photon correlation spectroscopy reveals intermittent aging dynamics in a metallic glass. *Phys. Rev. Lett.* **115,** 175701 (2015).

25. Fan, Y., Iwashita, T. & Egami, T. Crossover from localized to cascade relaxations in metallic glasses. *Phys. Rev. Lett.* **115,** 045501 (2015).

26. Leocmach, M. & Tanaka, H. Roles of icosahedral and crystal-like order in the hard spheres glass transition. *Nat. Commun.* **3,** 974 (2012).

27. Conrad, J. C., Starr, F. W. & Weitz, D. A. Weak correlations between local density and dynamics near the glass transition. *J. Phys. Chem. B* **109,** 21235–21240 (2005).

28. Russo, J. & Tanaka, H. The microscopic pathway to crystallization in supercooled liquids. *Sci. Rep.* **2,** 505 (2012).

29. Goldstein, M. Viscous liquids and the glass transition: a potential energy barrier picture. *J. Chem. Phys.* **51,** 3728–3739 (1969).

30. Dyre, J. C. Solidity of viscous liquids. ii. anisotropic flow events. *Phys. Rev. E* **59,** 7243–7245 (1999).

31. Lematre, A. Structural relaxation is a scale-free process. *Phys. Rev. Lett.* **113,** 245702 (2014).

32. Gelin, S., Tanaka, H. & Lematre, A. Anomalous phonon scattering and elastic correlations in amorphous solids. *Nat. Mater.* **15,** 1177–1181 (2016).

33. Henkes, S. & Chakraborty, B. Statistical mechanics framework for static granular matter. *Phys. Rev. E* **79,** 061301 (2009).

34. Maxwell, J. C. On the calculaton of the equilibrium stiffness of frames. *Phil. Mag.* **27,** 294–299 (1865).

35. Rosales-Pelaez, P., Montero de Hijes, P., Sanz, E. & Valeriani, C. Avalanche mediated devitrification in a glass of pseudo hard-spheres. *J. Stat. Mech. Theory Exp.* **9,** 094005 (2016).

36. Zaccarelli, E. *et al.* Crystallization of hard-sphere glasses. *Phys. Rev. Lett.* **103,** 135704 (2009).

37. Sanz, E. *et al.* Crystallization mechanism of hard sphere glasses. *Phys. Rev. Lett.* **106,** 215701 (2011).

38. Donati, C. *et al.* Stringlike cooperative motion in a supercooled liquid. *Phys. Rev. Lett.* **80,** 2338–2341 (1998).

39. Weeks, J. D. Role of repulsive forces in determining the equilibrium structure of simple liquids. *J. Chem. Phys.* **54,** 5237–5247 (1971).

40. Zargar, R., Nienhuis, B., Schall, P. & Bonn, D. Direct measurement of the free energy of aging hard sphere colloidal glasses. *Phys. Rev. Lett.* **110,** 258301 (2013).

41. Lubachevsky, B. D. & Stillinger, F. H. Geometric properties of random disk packings. *J. Stat. Phys.* **60,** 561–583 (1990).

42. Ermak, D. L. & McCammon, J. A. Brownian dynamics with hydrodynamic interactions. *J. Chem. Phys.* **69,** 1352–1360 (1978).

43. Filion, L., Ni, R., Frenkel, D. & Dijkstra, M. Simulation of nucleation in almost hard-sphere colloids: the discrepancy between experiment and simulation persists. *J. Chem. Phys.* **134,** 134901 (2011).

44. Ahmed, A. & Sadus, R. J. Phase diagram of the Weeks-Chandler-Andersen potential from very low to high temperatures. *Phys. Rev. E* **80,** 061101 (2009).

45. Kawasaki, T. & Tanaka, H. Formation of a crystal nucleus from liquid. *Proc. Natl Acad. Sci. USA* **107,** 14036–14041 (2010).

46. Russo, J., Maggs, A. C., Bonn, D. & Tanaka, H. The interplay of sedimentation and crystallization in hard-sphere suspensions. *Soft Matter* **9,** 7369–7383 (2013).

47. Steinhardt, P. J., Nelson, D. R. & Ronchetti, M. Bond-orientational order in liquids and glasses. *Phys. Rev. B* **28,** 784–805 (1983).

48. Lechner, W. & Dellago, C. Accurate determination of crystal structures based on averaged local bond order parameters. *J. Chem. Phys.* **129,** 114707 (2008).

49. Kawasaki, T. & Tanaka, H. Structural origin of dynamic heterogeneity in three-dimensional colloidal glass formers and its link to crystal nucleation. *J. Phys. Condens. Matter* **22,** 232102 (2010).

50. Rycroft, C. H. VORO++: a three-dimensional Voronoi cell library in C++. *Chaos* **19,** 041111 (2009).

Acknowledgements

Author contributions

H.T. conceived and supervised the project, T.Y. performed the numerical simulations and analysis. J.R. wrote the BOO calculation packages. All authors discussed the results and contributed to the writing of the manuscript.

Additional information